Precision Clinical Medicine, 2024, **7**: pbae028
DOI: 10.1093/pcmedi/pbae028
Research Article

Targeted nuclear degranulation of neutrophils promotes the progression of pneumonia in ulcerative colitis

Yiming Shao [1,2,‡] Qibing Zheng,[2,‡] Xiaobei Zhang,[1,‡] Ping Li,[3,‡] Xingxin Gao,[4] Liming Zhang,[4] Jiahong Xu,[2] Lingchao Meng,[2] Yanyun Tian,[2] Qinqin Zhang,[2] Guangxi Zhou [1,*]

[1]Taishan Scholars Laboratory, Affiliated Hospital of Jining Medical University, Jining 272000, China
[2]Department of Burns and Plastic Surgery, Affiliated Hospital of Jining Medical University, Jining 272000, China
[3]Research Center for Neutrophil Engineering Technology, Affiliated Suzhou Hospital of Nanjing Medical University, Suzhou 215002, China
[4]Department of Burns and Plastic Surgery, First Affiliated Hospital of Guangxi Medical University, Nanning 530000, China
*Corresponding author: Guangxi Zhou, zgx_viola@126.com
‡Yiming Shao, Qibing Zheng, Xiaobei Zhang, and Ping Li contributed equally to this work.

Abstract

Background: Both intestinal and pulmonary systems are parts of the mucosal immune system, comprising ~80% of all immune cells. These immune cells migrate or are transported between various mucosal tissues to maintain tissue homeostasis.

Methods: In this study, we isolated neutrophils from the peripheral blood of patients and utilized immunofluorescence, flow cytometry, and Western blotting to confirm the incidence of "nucleus-directed degranulation" *in vitro*. Subsequently, we conducted a precise analysis using arivis software. Furthermore, using the DSS mouse model of colitis and tissue clearing technologies, we validated the "targeted nuclear degranulation" of neutrophils and their migration to the lungs in an inflammatory intestinal environment.

Result: In this study, we found that among patients with ulcerative colitis, the migration of neutrophils with "targeted nuclear degranulation" from the intestinal mucosa to the lungs significantly exacerbates lung inflammation during pulmonary infections. Notably, patients with ulcerative colitis exhibited a higher abundance of neutrophils with targeted nuclear degranulation. Using DSS mice, we observed that neutrophils with targeted nuclear degranulation from the intestinal mucosa migrated to the lung and underwent activation during pulmonary infections. These neutrophils rapidly released a high amount of neutrophil extracellular traps to mediate the progression of lung inflammation. Alterations in the neutrophil cytoskeleton and its interaction with the nuclear membrane represent the primary mechanisms underlying targeted nuclear degranulation.

Conclusion: This study revealed that neutrophils accelerate lung inflammation progression in colitis, offering new insights and potential treatment targets for lung infections for patients with colitis.

Keywords: neutrophils; targeted nuclear degranulation; reverse migration; ulcerative colitis; pneumonia

Graphical Abstract

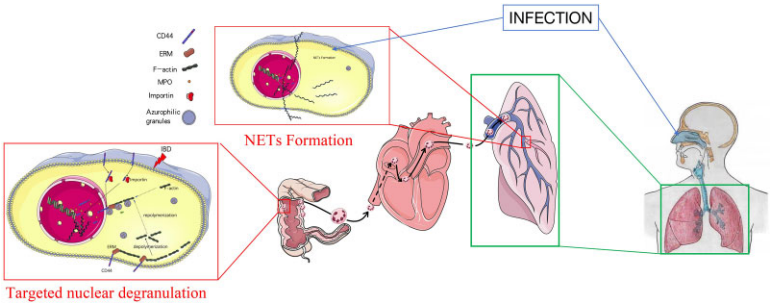

Targeted nuclear degranulation of neutrophils promotes the progression of pneumonia in ulcerative colitis.

Introduction

The phenomenon of pulmonary–intestinal crosstalk was initially documented in 1968 and validated in subsequent studies, particularly in relation to inflammatory bowel disease (IBD)-associated lung disorders [1, 2]. With the widespread use of high-resolution CT scanning, an increasing number of patients with IBD have been identified to have potential pulmonary dysfunction, even in the absence of overt symptoms [3, 4]. Typical pulmonary

Received 27 July 2024; revised 2 October 2024; accepted 12 October 2024. published 14 October 2024

manifestations of ulcerative colitis (UC) include airway and lung diseases, which often emerge months to years after the onset of UC [5–8]. The respiratory and gastrointestinal systems are integral components of the mucosal immune system, enabling the transfer of immune cells between different mucosal tissues [9].

The mucosal immune system encompasses ∼80% of all immune cells, which migrate between different mucosal tissues to maintain tissue homeostasis [10]. Neutrophils, the most abundant immune cells, will be activated after infection and migrate to the site of infection [11, 12]. Neutrophil extracellular traps (NETs), a novel form of neutrophil death, consist of DNA from the nucleus or mitochondria, anti-microbial peptides, and hydrolytic enzymes, forming a mesh-like structure [13]. However, numerous studies have reported that excessive release of NETs can damage the endothelium and accelerate the progression of several diseases [14, 15]. In a previous study, we discovered that targeted nuclear degranulation serves as a crucial mechanism for neutrophils to release NETs during sepsis [16]. We observed that azurophilic granules merge with the nucleus and release myeloperoxidase (MPO) into the nucleus, participating in the decondensation of nuclear proteins and the unwinding of DNA. Additionally, neutrophils undergoing targeted nuclear degranulation can exist in a pre-activation state in the circulation and rapidly form NETs after stimulation [16].

The excessive release of NETs in the lung during lung infections significantly accelerates disease progression [17–19]. In clinical practice, we noted that patients with active UC experience rapid deterioration of lung symptoms after lung infections. However, the specific underlying mechanism remains unclear. Our study uncovered that neutrophils with targeted nuclear degranulation in the intestinal mucosa of Dextran sulphate sodium (DSS) mice can enter the circulation and migrate to the lung during lung infections. These neutrophils rapidly release NETs after stimulation in the lung, thereby facilitating the progression of inflammation. These findings provide invaluable insights into the management of lung infections in patients with IBD and advance our understanding of pulmonary–intestinal crosstalk.

Materials and methods

Ethical statement

This study was approved by The Jining Medical University Committee. For experiments involving human blood samples, signed informed consent was obtained from all patients and healthy volunteers. Blood samples were taken from the cubital veins of patients and healthy donors. All the experimental methods were carried out in accordance with the approved guidelines. All experimental procedures involving mice were carried out in strict accordance with the recommendations in the Guide for the Care and Use of Laboratory Animals of the National Institutes of Health and State Key Laboratory of Pathogens and Biosecurity of the Institute of Microbiology and Epidemiology. Blood samples from patients with UC were obtained from the Affiliated Hospital of Jining Medical University, and blood samples from healthy individuals were obtained from the medical examination center.

Neutrophil extraction

A neutrophil isolation kit was used to isolate functional, highly purified neutrophils directly from human whole blood by immunomagnetic negative selection (STEMCELL Technologies, #18 103, #19 666). Briefly, 50 μl of liquid A and 50 μl of liquid B (magnetic beads) were added to each 1 ml blood sample, mixed and allowed to stand for 5 min. Stem buffer, diluted 1 : 1, was added to the blood sample, which was then placed in a magnetic rack and allowed to stand for 10 min. The supernatant was aspirated, 50 μl of solution B was added to each 1 ml of supernatant, and the mixture was again placed in the magnetic rack for 5 min. The supernatant was aspirated and placed in the magnetic rack for a further 5 min. The supernatant was then aspirated and centrifuged at 400 × g for 5 min to obtain neutrophils. Neutrophils were extracted and stored in RPMI-1640 medium (Gibco, Canada) containing 10% fetal calf serum (FBS).

Mice

Male mice (C57BL/6, 8 weeks old, Suzhou, China) were maintained at the Animal Experimental Center of Jining Medical University under a 12-h light–night cycle with free access to food and water for at least 1 week before the experiments.

A DSS-induced colitis model in mice was established using a method described previously [25, 26]. Briefly, wild type (WT) mice were given 2.0% DSS (molecular mass, 36 000–50 000, MP Biomedicals, Solon, OH, USA) in their drinking water for a continuous 7 days.

Chloral hydrate (8%) was injected intraperitoneally for anesthesia. The abdomen of the mouse was shaved and the abdominal skin disinfected. The abdominal cavity was opened in a sterile environment and the colon was located along the cecum. Prestained exogenous neutrophils were injected into the intestinal wall and the intestine was returned to the abdominal cavity. The abdomen was then closed layer by layer.

Quantification of MPO–DNA complexes

MPO–DNA complexes were quantified similarly to previously described protocols [28]. This protocol used several reagents from the Cell Death Detection Enzyme-Linked Immunosorbent Assay (ELISA) kit (Roche). First, a high-binding EIA/RIA 96-well plate (Costar) was coated overnight at room temperature (RT) with anti-human MPO antibody (RD, DY DY3174). The plate was washed twice with wash buffer [0.05% Tween-20 in phosphate-buffered saline (PBS)] and then blocked with 4% bovine serum albumin (Millipore Sigma) in PBS (with 0.05% Tween-20) for 1 h at RT. The plate was again washed five times before incubating for 90 min at RT with serum or plasma. The plate was washed a further five times and then incubated for 90 min at RT with anti-DNA antibody (Horseradish Peroxidase (HRP) conjugated; from the Cell Death kit). After five more washes, the plate was developed with 3, 3′,5 ,5′-Tetramethylbenzidine (TMB) followed by a 1 M sulfuric acid stop solution. Absorbance was measured at a wavelength of 450 nm using a Cytation 5 Cell Imaging Multi-Mode Reader (BioTek).

Nucleoprotein and cytoplasmic protein extraction

Nucleoproteins and cytoplasmic proteins were extracted with nuclear and cytoplasmic extraction reagents (Thermo, 78 835) according to the supplied protocol. Briefly, the treated cells were washed twice with prechilled PBS and centrifuged at 500 × g for 3 min. The cells were resuspended in 200 μl of cytoplasmic extraction reagent I. The suspension was incubated on ice for 10 min, 11 μl of cytoplasmic extraction reagent II was added, incubated on ice for 1 min and then centrifuged at 16 000 × g for 5 min. The supernatant fraction (cytoplasmic extract) was transferred to a prechilled tube. The insoluble precipitated fraction, containing the crude nuclei, was resuspended in 100 μl of nuclear extraction reagent and incubated on ice for 10 min, followed by

centrifugation at 16 000 × g for 10 min. The resulting supernatant contained the nucleoproteins. After extraction, the nuclear and cytoplasmic proteins were stored at −80°C until use.

Western blot analysis

The extracted proteins were separated by Sodium Dodecyl Sulfate Polyacrylamide Gel Electrophoresis (SDS-PAGE) on 7.5%–12% polyacrylamide gels and stained with Coomassie blue. The following primary antibodies were used: anti-MPO (Abcam, ab208670, 1 : 1000), anti-CD63 (Abcam, ab271286, 1 : 1000), and anti-laminB1 (Abcam, ab16048, 1 : 1000).

Immunostaining and microscopy

Cells were fixed in 4% paraformaldehyde, permeabilized with 0.1% Triton X-100, blocked with 5% BSA, and stained with the following: anti-citrullinated histone H3 (citH3) (Abcam, ab219407; 1 : 1000), anti-MPO (Abcam, ab208670; 1 : 100), anti-laminB1 (Abcam, ab16048; 1 : 1000), and anti-CD63 (Abcam, ab227892; 1 : 1000) primary antibodies; 4',6-diamidino-2-phenylindole (DAPI) (Solarbio D6470) was used for staining. After staining, the cells were observed using a Zeiss LSM 900 confocal microscope. Arivis software was used for processing 3D images.

Flow cytometry

Neutrophils purified from patients and healthy donors were stained with anti-CD63 (PE, BioLegend, 353 010), anti-CD35 (FITC, BD, 565 330), TdT-mediated dUTP Nick-End Labeling (TUNEL) (V450, BD, 561 425), annexin V PE/7-aminoactinomycin D (7-AAD) (BD, 559 763), and Chloromethyl-2',7'-Dichlorodihydrofluorescein Diacetate (CM-H2DCFH-DA) (FITC, Solarbio, D6470). Respiratory oxygen explosion of neutrophils was detected using CM-H2DCFDA (Solarbio, China). After being stimulated by 10 nM Phorbol 12-myristate-13-acetate (PMA) (Solarbio, China) for 30 min, neutrophils were stained with 10 mM H2DCFDA in a 37°C incubator for 30 min followed by washing twice in PBS before analysis. To detect apoptosis, antibodies, annexin V, and 7-AAD (BD Bioscience, USA) were added following the manufacturer's protocol. After incubating for 15 min at RT in the dark, the neutrophils were assessed.

Immunohistochemistry

Tissue was fixed in 4% formaldehyde, paraffin-embedded, and sectioned at 5 μm. The sections were exposed to 3% hydrogen peroxide for 10 min to inhibit endogenous peroxidase activity, followed by blocking with 3% bovine serum albumin for 30 min. The tissue sections were stained with hematoxylin and eosin and then observed by light microscopy.

Tissue sections were prepared as described above and incubated with Ly6G antibody (Abcam, ab238132; 1 : 2000) at 4°C overnight. The sections were then washed and incubated with anti-rabbit IgG secondary antibody for 30 min at RT. Then, the sections were restained with hematoxylin and developed using a diaminobenzidine kit. Results were obtained by examination under an IX73 microscope (Olympus).

Tissue sections were prepared as previously described [29]. The sections were then incubated overnight with rabbit anti-citH3 antibody (Abcam, ab219407, 1 : 100) and rabbit anti-MPO polyclonal antibody (Abcam, ab208670, 1 : 100). After washing, the slides were incubated with fluorescent dye-coupled secondary antibodies for 1 h at RT. The DNA was stained with DAPI (Servicebio, G1012, 1:200) for 10 min. Images were acquired using a fluorescence microscope.

ELISA

The procedure was carried out based on a kit protocol: MPO (RD, DY9167-05, DY3174), soluble thrombomodulin (sTM) (Elabscience, E-EL-H0166c), MPO activity (Sigma, MAK068). Then, 50–100 μl volumes of standards or samples were added to a 96-well plate and incubated at RT. Samples were added to three wells each. Biotinylated antibody, streptavidin-HRP reagent, and TMB substrate were added sequentially according to the protocol. Color was developed by incubation for 5–30 min at RT while the sample was protected from light. Stop solution was added to each well. The absorbance at the protocol required was measured within 5 min to measure protein levels, and the data were recorded.

iDISCO + tissue clearing

The mice were placed under deep anesthesia with 2% isoflurane and then perfused with 20 ml of PBS and 20 ml of 4% paraformaldehyde (PFA)/PBS solution. Lungs were quickly harvested and fixed in 4% PFA/PBS at 4°C overnight and then post-fixed for 1 h at RT. Lungs were stored in PBS at 4°C for further processing. For tissue clearing, we used the iDISCO + method as described online (https://idisco.info/) with slight modification [20]. For pretreatment, lungs were washed in PBS at room temperature three times, 30 min each. The lungs were dehydrated at room temperature by gradient methanol aqueous solutions (20%, 40%, 60%, 80%, and 100%, 1 h each). For a final removal of any residual water, the lungs were washed in 100% methanol solution for an additional 2 h. After dehydrating, lungs were incubated in 66% dichloromethane/methanol solution overnight at RT and then washed in 100% methanol for 2 h. Lungs were bleached overnight at 4°C in 5% H_2O_2/methanol solution and then rehydrated in a series of methanol solutions (80%, 60%, 40%, and 20%, PBS; 1 h each). After PBS treatment, lungs were washed in 0.2% Triton X-100 in PBS (PBS-T) twice (1 h each). Finally, the lungs were washed overnight, dehydrated, and then washed in 100% methanol overnight to remove residual water. Next day, lungs were washed in 66% dichloromethane/methanol solution for 3 h at room temperature and 100% dichloromethane twice, each for 30 min. Finally, the lungs were incubated in 100% dibenzyl ether until they looked transparent.

The transparent lungs were placed in a chamber filled with dibenzyl ether and were imaged by using the Zeiss light-sheet7 microscope. The 488 laser power was set at 95% to scan the whole lung.

Statistical analyses

All statistical analyses were performed and graphs were prepared with GraphPad Prism 8.0 software and Adobe Illustrator. 3D image processing was carried out using arivis software. The Shapiro–Wilk test was used to test the normality of continuous variables. The results are expressed as the mean ± standard deviation (SD). For group comparisons, one-way Analysis of Variance (ANOVA) was used to compare continuous variables with a normal distribution. The Kruskal–Wallis test was used to compare continuous variables with a skewed distribution. Tukey's *post hoc* test or Dunn's *post hoc* test was used for multiple comparisons. Student's t test and the Wilcoxon paired signed rank test were used to compare differences between two groups. The Pearson correlation coefficient was used for correlation analysis. Significant differences are denoted by asterisks ($^{*}P < 0.05$, $^{**}P < 0.01$, $^{***}P < 0.001$, $^{****}P < 0.0001$).

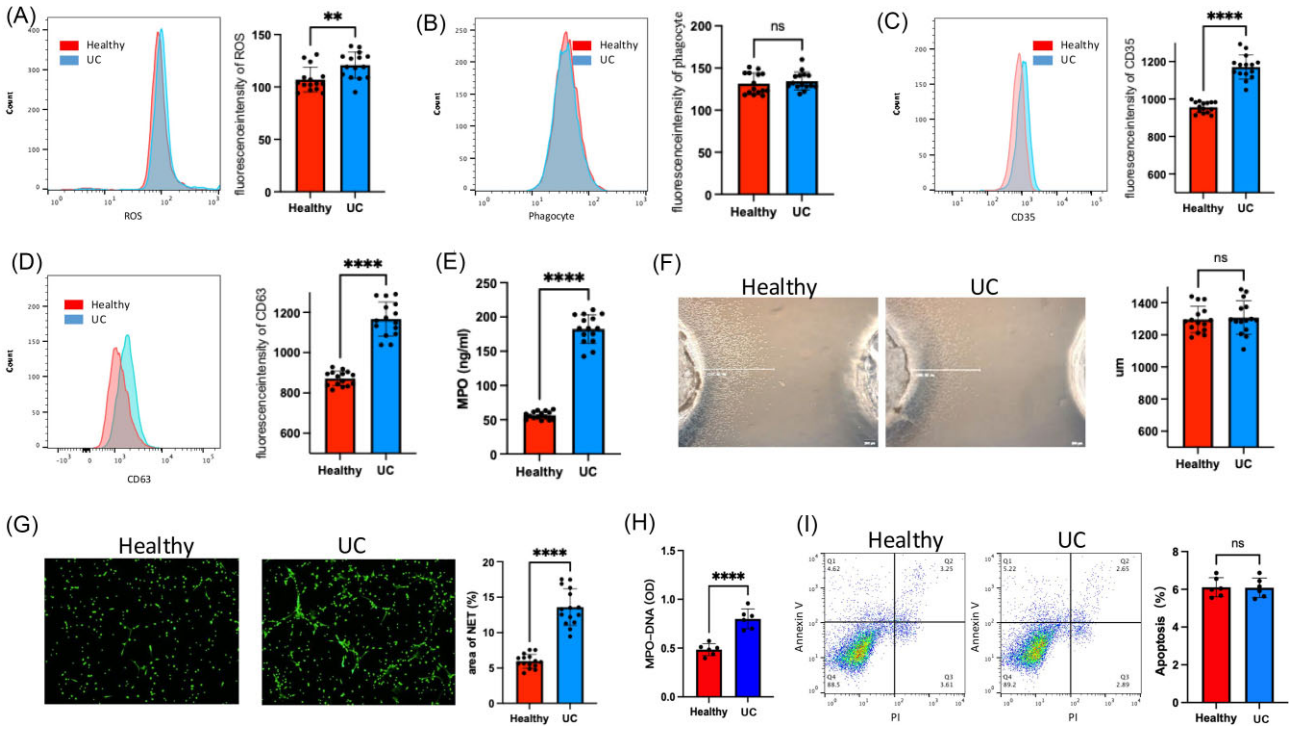

Figure 1. Partial dysfunction of neutrophils in patients with UC. (**A**) Flow cytometry analysis showed significant difference in ROS release of neutrophils between patients and volunteers. (**B**) Flow cytometry analysis showed no significant difference in phagocytic ability of neutrophils between patients and volunteers. (**C, D**) Flow cytometry analysis of CD35 and CD63 expression on neutrophils from both groups showed increased degranulation in patient neutrophils. (**E**) ELISA detected higher levels of MPO in the peripheral blood plasma of patients compared to volunteers. (**F**) Chemotaxis assay showed no significant difference in the chemotactic function of neutrophils between the two groups. (**G**) Neutrophils from patients released more NETs when stimulated with LPS *in vitro* for 60 min. (**H**) ELISA detected increased expression of MPO–DNA (NETs) in the peripheral blood plasma of IBD patients. (**I**) Flow cytometry analysis showed no significant difference in neutrophil apoptosis rate between the two groups after 24 h. ns, Not significant.

Results

Partial dysfunction of neutrophils in patients with UC

We isolated peripheral blood neutrophils from 15 healthy volunteers and 15 individuals with UC and conducted *in vitro* experiments to assess their function. Our findings indicate no significant changes in the ability of neutrophils from patients with UC to release reactive oxygen species (ROS) or perform phagocytosis (Fig. 1A, B). However, there was a significant increase in neutrophil degranulation (Fig. 1C, D) and MPO level in the peripheral blood (Fig. 1E). Further experiment revealed that among patients with UC, neutrophils exhibited granule polarization and had stronger MPO activity in peripheral blood (Fig. S1A, B, see online supplementary material). Using our newly developed neutrophil chemotaxis model, we observed no significant alterations in the chemotaxis of neutrophils from patients with UC (Fig. 1F). Furthermore, Lipopolysaccharide (LPS) stimulation led to a greater release of NETs from the peripheral blood neutrophils of patients with UC compared to healthy individuals (Fig. 1G). Additionally, the content of MPO–DNA complexes, a marker of NETs, was significantly increased in the peripheral blood of patients with UC (Fig. 1H). Finally, the apoptosis of neutrophils in patients with UC did not exhibit a significant delay (Fig. 1I). Patients with UC had increased neutrophil degranulation in peripheral blood and a greater tendency to release NETs.

Targeted nuclear degranulation of neutrophils is enhanced in patients with UC

Neutrophils were isolated from the peripheral blood of five individuals with UC and five healthy individuals. TUNEL staining revealed a significant increase in DNA fragmentation within the neutrophil nuclei of patients with UC (Fig. 2A, B). Moreover, Peptidylarginine deiminase (PAD) activity (citH3) was significantly upregulated in the nuclei of neutrophils in patients with UC (Fig. 2C). In addition, the expression of citH3 was significantly elevated in the plasma of patients (Fig. 2D). Increased nuclear entry of MPO was identified as the main cause of nuclear DNA breakage. Notably, patients with UC exhibited a significant increase in MPO activity in the nuclei of neutrophils (Fig. 2E, F, and Fig. S2A, Movie 1, 2, see online supplementary material). Electron microscopy revealed fusion between the granules and nuclear membrane in the neutrophils of patients with UC (Fig. 2G). Furthermore, staining for neutrophil granule membrane (CD63) and nuclear membrane (laminB) demonstrated a significant increase in co-localization between the granule membrane and nuclear membrane among patients with UC (Fig. 2H, I). Two hours after culturing neutrophils from patients with UC, the intranuclear MPO in the neutrophils of patients with UC was not decreased and the expression of nuclear membrane CD63 was not reduced (Fig. S2B, C).

Our previous study unveiled that targeted nuclear degranulation is an intermediate state of neutrophil activation. In this study,

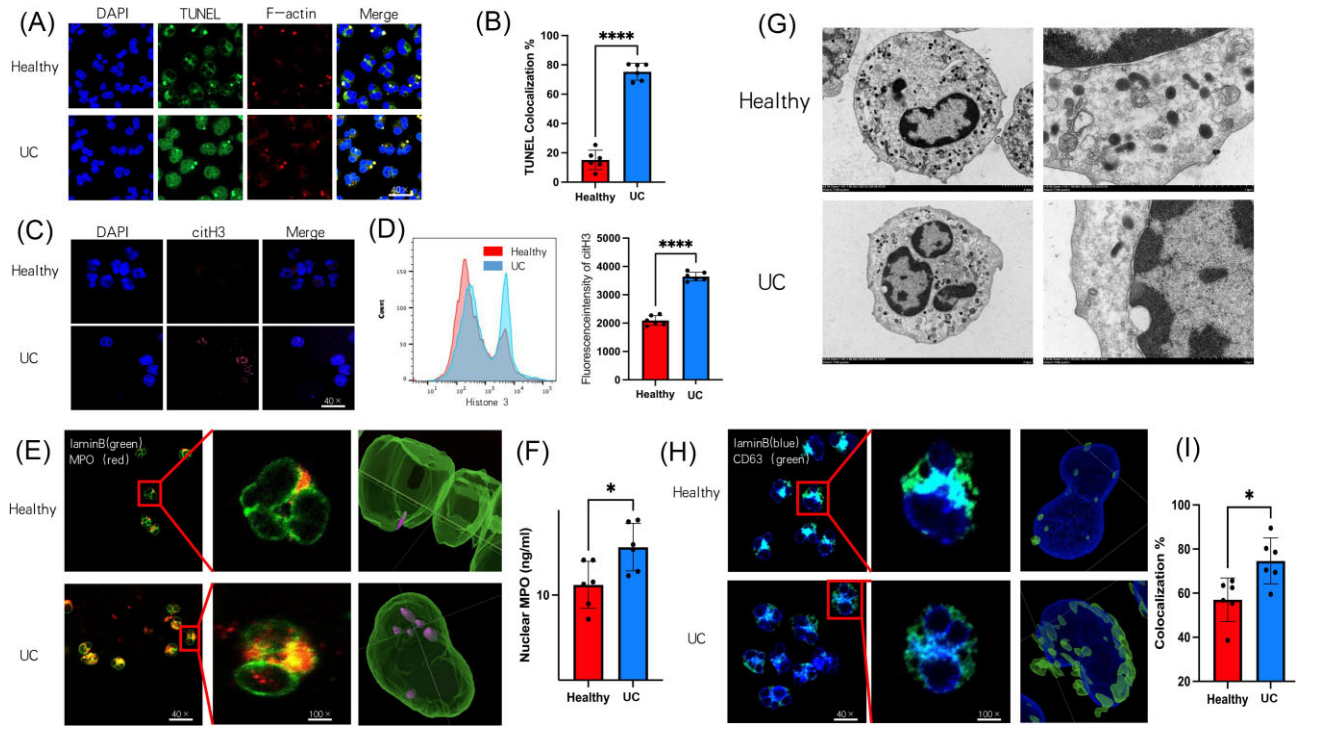

Figure 2. Targeted nuclear degranulation of neutrophils is enhanced in patients with UC. (**A**) Increased nuclear DNA fragmentation (TUNEL) in neutrophils from IBD patients. (**B**) Increased co-localization of TUNEL (DNA breaks) and nuclear staining (DAPI) in neutrophils from IBD patients. (**C**) Increased expression of citH3 in the nuclei of neutrophils from IBD patients. (**D**) Flow cytometry analysis showing increased expression of free citH3 in peripheral blood of IBD patients. (**E**) Immunofluorescence staining for MPO (red) and nuclear membrane (laminB, green) showing increased nuclear MPO in neutrophils from IBD patients. (**F**) Nuclear protein extraction followed by ELISA showing increased nuclear MPO expression in neutrophils from IBD patients. (**G**) Electron microscopy revealing fusion of granules with the nuclear membrane in neutrophils from IBD patients. (**H, I**) Immunofluorescence staining for eosinophilic granules (CD63, green) and nuclear membrane (laminB, blue) showing increased co-localization of granules and nuclear membrane in neutrophils from IBD patients.

we found a significant increase in neutrophil targeted nuclear degranulation in the peripheral blood of patients with UC, which may be the reason for the increased release of NETs in patients with UC.

Intestinal targeted nuclear degranulation neutrophils migrate to the lung

Our findings indicated that patients with UC have an increased abundance of neutrophils undergoing targeted nuclear degranulation in the peripheral blood circulation. Furthermore, *in vitro* stimulation enhanced the release of NETs. Therefore, we hypothesized that neutrophils with targeted nuclear degranulation originate from the intestinal inflamed mucosa and can re-enter the lung through the peripheral blood circulation (Fig. 3A). We injected exogenous neutrophils (red) into the intestinal mucosa of DSS mice and simultaneously stained the mesenteric blood vessels (green). Confocal microscopy indicated neutrophils migrating in reverse toward the blood vessels (Fig. 3B, and Movie 3, see online supplementary material). After 6 h, we harvested the lungs of mice for transparency treatment. Immunofluorescence staining showed that neutrophils injected into the colon wall entered the lungs and were evenly distributed (Fig. 3C, and Movie 4, see online supplementary material). Using flow cytometry, we detected neutrophils injected through the intestine in the peripheral blood of mice. Among these neutrophils, we identified cells with a reverse migration phenotype ($ICAM1^{high}$, $CXCR1^{low}$) [21] (Fig. 3D). We first stained the cell membrane of neutrophils from WT mice, and then injected these neutrophils into the colonic mucosa of DSS mice and WT mice. After 6 h, we observed detectable neutrophils in the lungs of both endogenous and exogenous groups. There was no significant difference between them (Fig. 3E). Additionally, the expression of citH3 (red) was increased in intestinal neutrophils (purple) migrating to the lung of DSS mice, but the original neutrophils (green) in the lung did not express citH3 (red) (Fig. 3F). Furthermore, we collected and extracted neutrophils from the lung lavage of both groups of mice and found no difference in the number of neutrophils (red) from the intestine (Fig. 3G). However, the expression of MPO and nuclear membrane CD63 significantly increased in neutrophils from the lungs of DSS mice compared to WT mice (Fig. 3H). Moreover, we observed a significant increase in the co-localization of granule membrane (green) and nuclear membrane (blue) in neutrophils (red) from the intestine in the lung lavage of DSS mice compared to WT mice (Fig. 3I, Fig. S3A, see online supplementary material). Finally, we measured the lung lavage and found no significant difference in the expression of inflammatory factors between the two groups (Fig. S3B). Neutrophils in the intestinal mucosa can return to the circulation and migrate to the lungs. However, in DSS mice, neutrophils returning to the lungs exhibited stronger targeted nuclear degranulation.

DSS mice with pulmonary infection exhibit more severe pulmonary inflammation

We employed the DSS mouse model and administered LPS through the intranasal route. After 6 h, we obtained the lungs of the mice and observed no significant difference in the number of neutrophils between the lungs of DSS mice and the lungs of

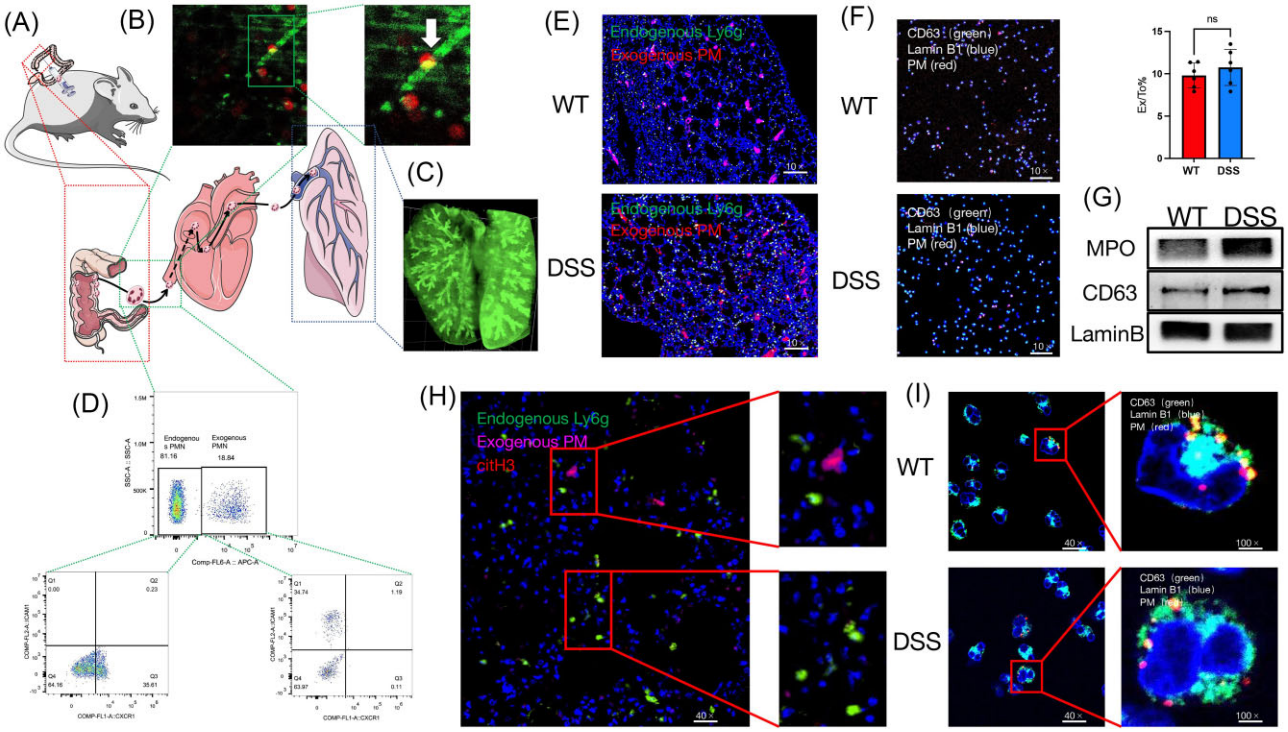

Figure 3. Intestinal targeted nuclear degranulation neutrophils migrate to the lung. (**A**–**C**) The intestinal mucosa of DSS mice was injected with exogenous neutrophils (red) and simultaneously stained with intestinal mesenteric vessels (green). (**B**) Neutrophils were observed to migrate towards the blood vessels under confocal microscopy. (**C**) The lung tissue transparency reveals a uniform distribution of neutrophils originating from the colon. (**D**) Using flow cytometry, we detected neutrophils injected through the intestine in the peripheral blood of mice. Within these neutrophils, we identified cells with a reverse migration phenotype ($ICAM1^{high}$, $CXCR1^{low}$). (**E**) Neutrophils from the intestine were detected in both normal mouse and DSS mouse lung (red). (**F**) After lung lavage, neutrophils were extracted from the lavage fluid. The proportion of neutrophils from the intestine wall was similar in the lungs of both groups of mice. (**G**) Increased MPO expression in the nuclei of neutrophils and increased nuclear membrane CD63 expression were observed in the bronchoalveolar lavage fluid of DSS mice. (**H**) Neutrophils from normal mice were fluorescently stained (green) and intravenously injected to simulate circulating neutrophils in the body. After collecting the lung, citH3 staining (red) shows that citH3 is primarily expressed in neutrophils derived from the intestine. (**I**) Immunofluorescence staining of neutrophils in the bronchoalveolar lavage fluid showed increased fusion of toluidine blue granules (red) from the intestinal neutrophils with nuclear membranes (laminB, blue) in DSS mice.

WT mice (Fig. 4A). Furthermore, there was no notable difference in the number of neutrophils in the bronchoalveolar lavage fluid between the two groups (Fig. 4B). The lung wet-to-dry ratio was higher in the DSS group compared to the WT group (Fig. 4C). In addition, we measured the presence of inflammatory factors in the bronchoalveolar lavage fluid and found a higher expression level of inflammatory factors [interleukin-6 (IL6) and IL17A] in the DSS group compared to the WT group (Fig. 4D). The mouse oxygenation index was significantly reduced in the DSS group compared to the WT group (Fig. 4E). Therefore, we found that DSS mice had more severe symptoms and progressed faster after lung infection compared to WT mice. Concurrently, the expression and activity of MPO were increased in the DSS group compared to the WT group (Fig. 4F, G). Neutrophils from the DSS group exhibited a higher level of NETs expression in the lung compared to the WT group (Fig. 4I). The expression of NETs was also significantly increased in the bronchoalveolar lavage fluid (Fig. 4H). To determine whether neutrophils releasing NETs primarily originated from the colon, we pre-stained neutrophils (purple) injected into the colon mucosa and found that these neutrophils expressed more citH3 (red) in the lungs (Fig. 4J). These findings revealed that those neutrophils with targeted nuclear degranulation from the colon of DSS mice migrated to infected lungs where they rapidly released NETs and worsened the symptoms of DSS mice. Seven days after modeling DSS mice, we began to continuously record the body weight and mortality rate of each mouse for 7 days. LPS stimulation of the lungs resulted in an increased mortality rate and significant weight loss in DSS mice (Fig. S4A, B, see online supplementary material).

Membrane fusion and cytoskeleton changes mediate targeted nuclear degranulation

In a previous study, we observed the occurrence of targeted nuclear degranulation and elucidated the underlying mechanisms [16]. In this study, we utilized neutrophils from human peripheral blood and conducted further experiments. Since the fusion of cell membranes is responsible for this phenomenon, we employed dexamethasone (DXMS) to stabilize the membrane. We uncovered that DXMS can effectively inhibit the co-localization of CD63 granules and the nuclear membrane (Fig. 5A, B). DXMS effectively inhibited MPO translocation to the nucleus and the formation of NETs (Fig. S4A, B). DXMS inhibited membrane fusion, effectively preventing nuclear DNA breakage (Fig. 5C). This finding indicated that the fusion of azurophilic granules with the nuclear membrane is one of the important mechanisms for the formation of NETs. *In vitro*, we stimulated neutrophils with PMA to simulate the release of NETs. We observed that cytochalasin, an inhibitor of cytoskeleton aggregation, effectively reduced the formation of NETs in neutrophils (Fig. 5D, and Movie 5, 6, see online supplementary material). Furthermore, after stimulating neutrophils with LPS for

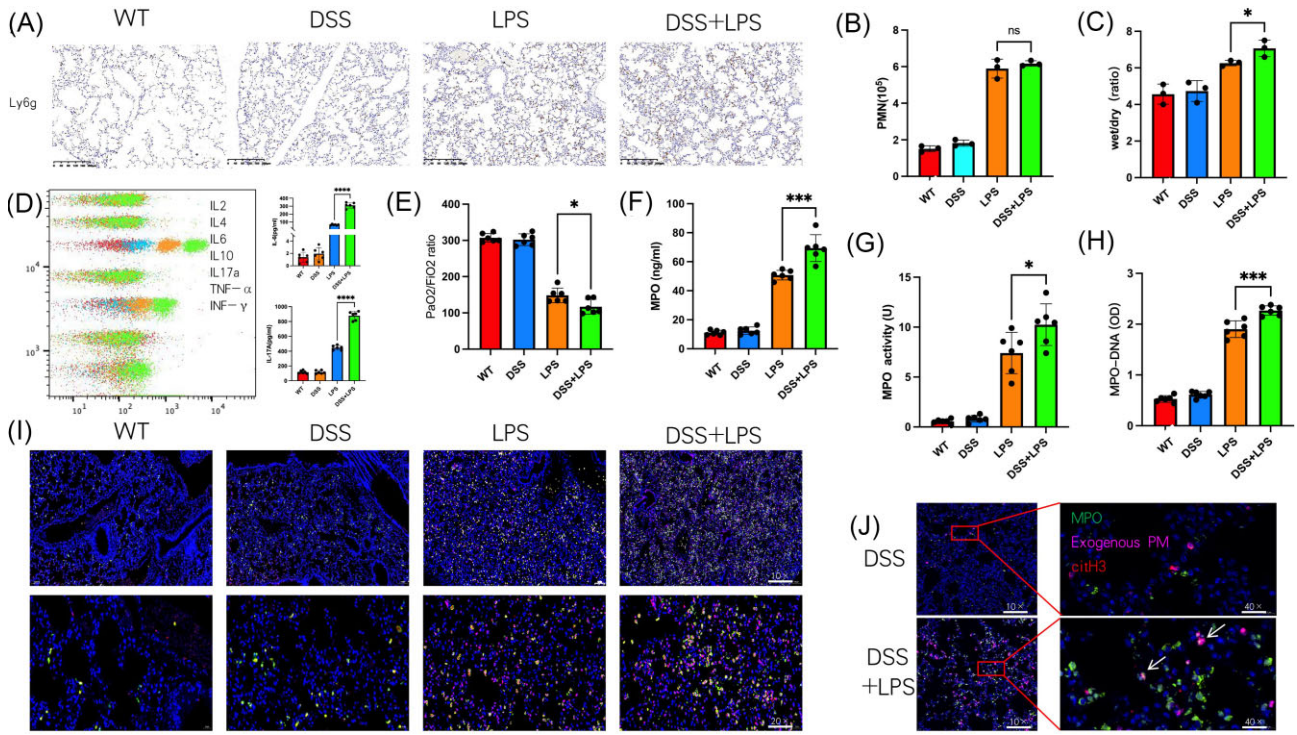

Figure 4. DSS mice with pulmonary infection exhibit more severe pulmonary inflammation. (**A**) LPS causes significant infiltration of neutrophils in the lung of both WT mice and DSS mice, but it causes more significant lung edema in DSS mice. (**B**) LPS leads to an increase in neutrophil counts in the bronchoalveolar lavage fluid of both groups of mice, with no significant difference. (**C**) LPS leads to a more significant dry-to-wet ratio in the lung of DSS mice. (**D**) LPS causes a significant increase in inflammatory factors (IL6, IL17A) in the bronchoalveolar lavage fluid of DSS mice. (**E**) LPS significantly decreases the oxygenation index in DSS mice. (**F**, **G**) LPS causes a greater increase in both MPO content and activity in the bronchoalveolar lavage fluid of DSS mice. (**H**, **I**) LPS leads to the generation of more NETs (MPO, green; +citH3, red) in the lung of DSS mice. (**J**) LPS significantly decreases the oxygenation index in DSS mice.

1 h, we found that both cytochalasin and the CD44 transport protein inhibitor, importini, effectively reduced the translocation of MPO into the nucleus (Fig. 5E). Therefore, we believe that the fusion of azurophilic particles with the nuclear membrane and the changes in the skeleton are important mechanisms underlying targeted nuclear degranulation.

CD44 mediates targeted nuclear degranulation during nuclear translocation of neutrophils

CD44, located on the surface of neutrophils, can serve as a link between F-actin and the cell membrane via ezrin/radixin/moesin (ERM) proteins. Upon activation, CD44 is released from the cell membrane (Fig. 6A). Our findings indicated that after neutrophil activation, CD44 is shed into the cytoplasm and then translocated to the nuclear membrane with the help of importin (a transfer protein) (Fig. 6B, C). Additionally, our study revealed that hindering cytoskeletal alterations and CD44 translocation to the nucleus can prevent the formation of NETs (Fig. 6D). Moreover, inhibiting the activity of importin reduces CD44 translocation to both the cytoplasm and nuclear membrane (Fig. 6E, F). We used a dynein inhibitor (dynarrestin) to suppress the movement of granules along the cytoskeleton toward the nucleus (Fig. 6G, and Fig. S5A, see online supplementary material). Dynarrestin effectively inhibited the co-localization of dynein (CD63, green) with F-actin (red). Similarly, dynarrestin effectively inhibited the co-localization of granules (CD63, green) with F-actin (red) (Fig. 6H). Moreover, dynarrestin effectively inhibited the formation of NETs induced after exposure to LPS (Fig. S5B). We also observed that dynarrestin effectively inhibited the increase in nuclear MPO levels after exposure to LPS (Fig. 6I). CD44 migrated to the nucleus and re-linked with F-actin at the nuclear membrane, which is an important mechanism mediating the proximity of azurophilic granules to the nucleus. Azurophilic granules approach the nuclear membrane through dynein on F-actin.

Discussion

In clinical practice, we observed that patients with active UC exhibit more severe pulmonary inflammation after lung infection. We speculated that this may be related to gut–lung immune crosstalk. Recent studies have suggested that the migration of immune cells in the mucosal immune system to different tissues is a key mechanism involved in gut–lung crosstalk [10, 22]. The discovery of neutrophils migrating in reverse supports this phenomenon [23]. Therefore, we focused on neutrophils, considering their abnormal function and migration as a reason behind the exacerbation of pulmonary diseases among patients with intestinal inflammation.

We also found that the partial function of neutrophils in the peripheral blood of patients with UC was abnormal. The degranulation markers of neutrophils showed a significant increase in the peripheral blood of patients with UC, possibly due to partial granule release at the site of colitis. Contrary to most of the previous reports, ROS release did not increase in this study [24, 25]. After staining with the DCFH-DA probe *in vitro*, no discernible secondary activation was observed. Similarly, we did not observe any significant abnormalities in phagocytic function, chemotaxis, and apoptosis in purified neutrophils. Interestingly, after stimulating neutrophils with LPS, UC neutrophils released more NETs. We speculated that the neutrophils of patients with UC were more easily

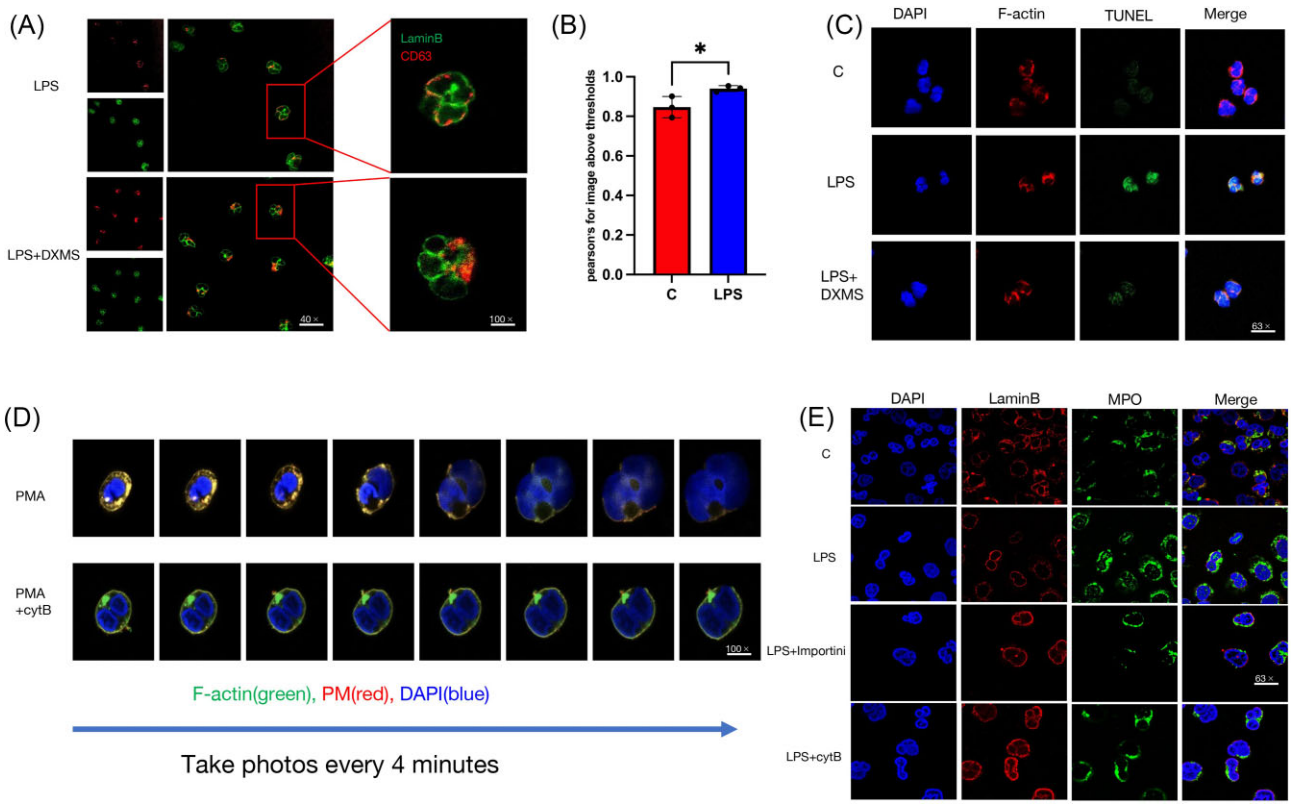

Figure 5. Membrane fusion and cytoskeleton changes mediate targeted nuclear degranulation. (**A**, **B**) Neutrophils were preincubated with DXMS for 15 min, and fluorescence staining shows that DXMS significantly inhibits the colocalization of CD63 with the nuclear membrane. (**C**) Dexamethasone significantly inhibits the breakage of nuclear DNA (TUNEL). (**D**) PMA stimulation induces NETs formation in neutrophils, and cytochalasin B (cytB) significantly inhibits NETs formation and neutrophil cytoskeleton changes. (**E**) Both cytB and importin activity inhibitors can inhibit the nuclear translocation of MPO.

activated. In our previous studies, we observed the phenomenon of neutrophil targeted nuclear degranulation and considered it as a mechanism for the release of NETs by neutrophils [16].

To verify the phenomenon of neutrophil targeted nuclear degranulation among patients with UC and its irreversibility, we first investigated whether neutrophils in the peripheral blood of patients with UC exhibit the targeted nuclear degranulation phenomenon. We measured the DNA fragmentation of neutrophils in the peripheral blood of patients with UC, MPO translocation into the nucleus, and CD63 (azurophilic granule membrane) fusion with the nuclear membrane. We observed membrane fusion under electron microscopy, confirming the existence of degranulation in the nucleus. Interestingly, Metzler *et al.* found that MPO did not enter the nucleus during the release of NETs [26]. Therefore, we optimized the analysis method using arivis software for immunofluorescence and confirmed MPO translocation into the nucleus. To confirm that MPO translocation into the nucleus is not easily reversible, we cultured neutrophils from patients with UC for 2 h, detected nuclear MPO again, and extracted nuclear membranes to detect CD63 expression, finding that targeted nuclear degranulation was not reversed. Without further stimulation, nuclear MPO was not expelled from the nucleus. Based on these findings, we speculated that neutrophil-targeted nuclear degranulation may represent a semi-activated state.

For the first time, Mathias *et al.* observed the reverse migration of zebrafish neutrophils from the site of inflammation back into the vascular system and introduced the concept of "reverse neutrophil migration". They suggested that reverse neutrophil migration is also an important pathway to neutrophil activation [12]. Compared to neutrophils in resident tissues and circulation, neutrophils undergoing reverse migration exhibit a unique phenotype. The neutrophil phenotype after reverse migration was cell ICAM-1^{high}, $CXCR1^{low}$, while neutrophils in resident tissue were ICAM-1^{low}, $CXCR1^{low}$, and the circulating neutrophils were ICAM-1^{low}, $CXCR1^{high}$ [21].

We verified whether these "semi-activated" neutrophils are the main components leading to lung–gut immune crosstalk. Using the DSS mouse model, we observed the presence of partially injected neutrophils in the mouse lungs after 6 h of injecting fluorescently labeled semi-activated neutrophils into the intestinal wall. To confirm that semi-activated neutrophils are an important factor exacerbating lung infection, we simultaneously injected semi-activated neutrophils and established a lung infection model in DSS mice (LPS). Similarly, after 6 h, we observed more severe respiratory symptoms in DSS mice and found that neutrophils of intestinal origin released more NETs in the lungs. However, the simple DSS mouse model may be incomplete, as this model provides more severe colitis and increases the risk of symptoms during lung infection. We will continue to improve the model in subsequent studies to provide more comprehensive evidence.

In general, mice with DSS-induced colitis are considered experimental models of UC, which exhibit clinical and histological features similar to human UC. Due to its simplicity, reproducibility, and controllability, the DSS colitis model in UC research has advantages over other experimental models of chemically induced UC [27]. Furthermore, transepithelial migration of neutrophils resulting in cryptitis and crypt abscess, a common histologic finding in UC, was reproduced in mice subjected to chronic DSS

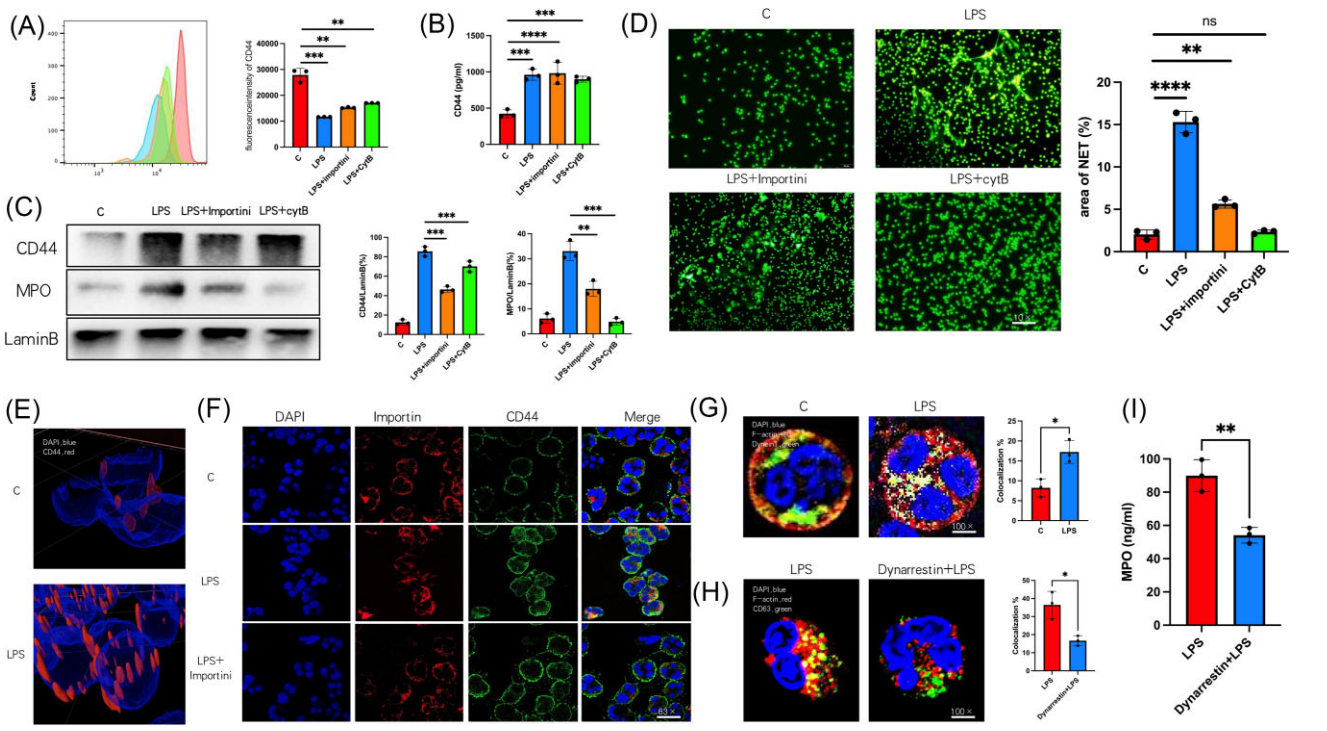

Figure 6. CD44 mediates targeted nuclear degranulation during nuclear translocation of neutrophils. (**A**) LPS stimulation resulted in the shedding of cell membrane CD44 in neutrophils, which was not inhibited by the cytB and importin activity inhibitor. (**B**) ELISA showed that LPS can stimulate the shedding of CD44 into the cytoplasm. (**C**, **E**, **F**) The importin activity inhibitor (importini) effectively inhibited the nuclear translocation of CD44 and further suppressed the nuclear translocation of MPO. (**D**) The combination of cytB and importin activity inhibitor can effectively inhibit the formation of NETs. (**G**, **H**) After pre-incubating neutrophils with the dynein inhibitor (dynarrestin), stimulate the neutrophils with LPS for 1 hour. Dynarrestin can effectively inhibit (**G**) the co-localization of dynein1 (green) and cytoskeleton (F-actin, red), (**H**) the co-localization of azurophilic granules (CD63, green) and cytoskeleton (F-actin, red), and (**I**) MPO entry into the nucleus.

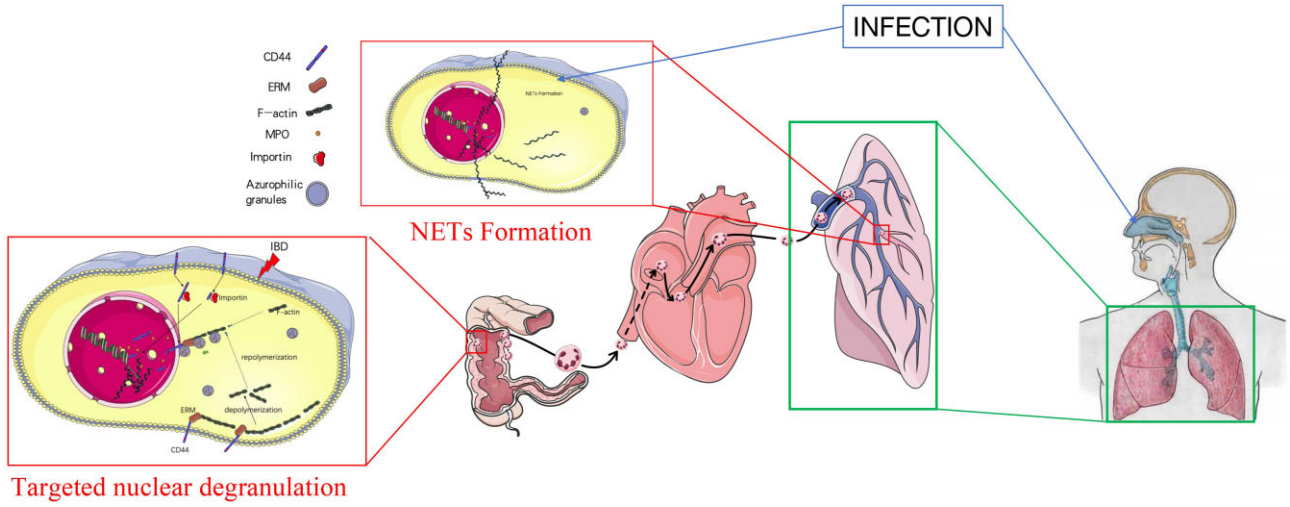

Figure 7. Targeted nuclear degranulation of neutrophils promotes the progression of pneumonia in UC. After receiving stimulation at the intestinal lesion site, neutrophils in the intestinal mucosa undergo cortical cytoskeleton depolymerization and reaggregation in the cytoplasm, while the cell membrane CD44 is shed into the cytoplasm and transported to the nucleus through importin protein. CD44 anchors F-actin to the nuclear membrane via ERM. Azurophilic granules move towards the nuclear membrane along F-actin and eventually fuse with the nuclear membrane to release MPO into the nucleus. When the lungs are infected, some of the intestinal neutrophils undergo "targeted nuclear degranulation" and reenter the circulation, eventually reaching the lungs. Neutrophils rapidly release large amounts of NETs in response to lung stimulation, exacerbating lung damage.

administration [28]. We injected the labeled neutrophils into the lesion site through the intestinal wall, which is different from the neutrophil infiltration of the intestinal wall in patients with UC. However, we primarily aimed to observe the process of neutrophil "reverse migration" from the intestinal wall. We also recognize the limitations of this model, and will optimize it in future studies. Numerous studies have shown that neutrophil reverse migration is a double-edged sword. On the one hand, neutrophil reverse

migration can promote the resolution of local inflammation by accelerating the clearance of neutrophils from local wounds. On the other hand, neutrophils re-enter the circulatory system, which may lead to the spread of systemic inflammation [29]. Our study also found that neutrophils in the intestinal lesion of patients with UC migrate in reverse to the infected lungs, increasing the symptoms of lung infections.

Although we observed targeted nuclear degranulation in neutrophils stimulated with PMA in our preliminary studies, this does not correspond to the pathogenesis of colitis, as in colitis, LPS is the main trigger for neutrophil activation. Therefore, we stimulated neutrophils with LPS, confirming the presence of targeted nuclear degranulation after LPS stimulation. Moreover, we found that CD44/ERM/F-actin formed on the nuclear membrane and the cytoplasmic dyneins carried azurophilic granules for transport on the cytoskeleton. This is the main mechanism of degranulation toward the nucleus. Additionally, we identified neutrophils with degranulation toward the nucleus in the peripheral blood of patients with UC. Hence, we believe that the retrograde pulmonary migration of neutrophils with degranulation toward the nucleus leads to severe lung infection in patients with colitis.

Our study unraveled that neutrophils with targeted nuclear degranulation in the intestinal mucosa of DSS mice can enter the circulation and migrate to the lung during lung infections. These neutrophils rapidly release NETs after stimulation in the lung, thereby facilitating the progression of inflammation (Fig. 7). These findings provide invaluable insights into the management of lung infections in patients with IBD and advance our understanding of pulmonary–intestinal crosstalk.

Acknowledgments

This work was supported by grants from the National Natural Science Foundation of China (Grants No. 82270562, 82302800), China Postdoctoral Science Foundation (Grant No. 2024M751108), Tai Shan Young Scholar Foundation of Shandong Province (Grant No. tsqn202103190), Postdoctoral Fund of The Affiliated Hospital of Jining Medical University (Grant No. JYFY364862), Postdoctoral Innovation Program in Shandong Province (Grant No. SDCX-ZG-202400032), and Doctor Fund of The Affiliated Hospital of Jining Medical University (Grant No. 2022-BS-07). The authors would like to express their gratitude to EditSprings (https://www.editsprings.cn) for the expert linguistic services provided.

Author contributions

Yiming Shao (Project administration, Visualization, Writing—original draft), Qibing Zheng (Conceptualization, Visualization), Xiaobei Zhang (Data curation, Investigation, Project administration, Writing—review & editing), Ping Li (Data curation, Resources), Xingxin Gao (Formal analysis, Validation), Liming Zhang (Methodology), Jiahong Xu (Investigation, Writing—original draft), Lingchao Meng (Data curation, Resources), Yanyun Tian (Formal analysis, Software), Qinqin Zhang (Methodology, Validation), and Guangxi Zhou (Writing—original draft).

Supplementary data

Supplementary data are available at *PCMEDI Journal* online.

Conflict of interest

None declared. Data is available from the authors upon reasonable request.

References

1. Turner-Warwick M. Fibrosing alveolitis and chronic liver disease. *Q J Med* 1968;**37**:133–49.
2. Dirks E, Goebell H, Eigler FW. The course and prognosis of ulcerative colitis. *Med Klin (Munich)* 1989;**84**:208–15.
3. Majima S, Wakahara K, Iwano S *et al.* Airway involvement in inflammatory bowel disease: inflammatory bowel disease patients have bronchial wall thickening. *Respir Investig* 2022;**60**:713–9. https://doi.org/10.1016/j.resinv.2022.06.003.
4. Bourdillon AT, Hajek MA, Wride M *et al.* Correlations of radiographic and endoscopic observations in subglottic stenosis. *Ann Otol Rhinol Laryngol* 2022;**131**:724–9. https://doi.org/10.1177/00034894211042768.
5. Camus P, Colby TV. The spectrum of airway involvement in inflammatory bowel disease. *Clin Chest Med* 2022;**43**:141–55. https://doi.org/10.1016/j.ccm.2021.12.003.
6. Tejeda Taveras N, Rivera Martinez A, Kumar R *et al.* Pulmonary manifestations of inflammatory bowel disease. *Cureus* 2021;**13**:e14216. https://doi.org/10.7759/cureus.14216.
7. Majewski S, Piotrowski W. Pulmonary manifestations of inflammatory bowel disease. *Arch Med Sci* 2015;**11**:1179–88. https://doi.org/10.5114/aoms.2015.56343.
8. Sun HY, Wang XY, Wu J. The interior-exterior correlation between fei and dachang from the lung function injury in ulcerative colitis patients. *Zhongguo Zhong Xi Yi Jie He Za Zhi* 2011;**31**:591–4.
9. Du B, Fu Y, Han Y *et al.* The lung-gut crosstalk in respiratory and inflammatory bowel disease. *Front Cell Infect Microbiol* 2023;**13**:1218565. https://doi.org/10.3389/fcimb.2023.1218565.
10. Mestecky J, Moldoveanu Z, Elson CO. Immune response versus mucosal tolerance to mucosally administered antigens. *Vaccine* 2005;**23**:1800–3. https://doi.org/10.1016/j.vaccine.2004.11.009.
11. Rosales C. Neutrophils at the crossroads of innate and adaptive immunity. *J Leukoc Biol* 2020;**108**:377–96. https://doi.org/10.1002/JLB.4MIR0220-574RR.
12. Mathias JR, Perrin BJ, Liu TX *et al.* Resolution of inflammation by retrograde chemotaxis of neutrophils in transgenic zebrafish. *J Leukoc Biol* 2006;**80**:1281–8. https://doi.org/10.1189/jlb.0506346.
13. Mutua V, Gershwin LJ. A review of neutrophil extracellular traps (NETs) in disease: potential anti-NETs therapeutics. *Clin Rev Allergy Immunol* 2021;**61**:194–211. https://doi.org/10.1007/s12016-020-08804-7.
14. Herre M, Cedervall J, Mackman N *et al.* Neutrophil extracellular traps in the pathology of cancer and other inflammatory diseases. *Physiol Rev* 2023;**103**:277–312. https://doi.org/10.1152/physrev.00062.2021.
15. Qu M, Chen Z, Qiu Z *et al.* Neutrophil extracellular traps-triggered impaired autophagic flux via METTL3 underlies sepsis-associated acute lung injury. *Cell Death Discov* 2022;**8**:375. https://doi.org/10.1038/s41420-022-01166-3.
16. Shao Y, Li L, Liu L *et al.* CD44/ERM/F-actin complex mediates targeted nuclear degranulation and excessive neutrophil extracellular trap formation during sepsis. *J Cell Mol Med* 2022;**26**:2089–103. https://doi.org/10.1111/jcmm.17231.
17. Zhang H, Liu J, Zhou Y *et al.* Neutrophil extracellular traps mediate m(6)A modification and regulates sepsis-associated acute

lung injury by activating ferroptosis in alveolar epithelial cells. *Int J Biol Sci* 2022;**18**:3337–57. https://doi.org/10.7150/ijbs.69141.
18. Keir HR, Chalmers JD. Neutrophil extracellular traps in chronic lung disease: implications for pathogenesis and therapy. *Eur Respir Rev* 2022;**31**:210241. https://doi.org/10.1183/16000617.0241-2021.
19. Scozzi D, Liao F, Krupnick AS *et al.* The role of neutrophil extracellular traps in acute lung injury. *Front Immunol* 2022;**13**:953195. https://doi.org/10.3389/fimmu.2022.953195.
20. Chang J, Guo B, Gao Y *et al.* Characteristic features of deep brain lymphatic vessels and their regulation by chronic stress. *Research (Wash D C)* 2023;**6**:0120. https://doi.org/10.34133/research.0120.
21. Buckley CD, Ross EA, McGettrick HM *et al.* Identification of a phenotypically and functionally distinct population of long-lived neutrophils in a model of reverse endothelial migration. *J Leukoc Biol* 2006;**79**:303–11. https://doi.org/10.1189/jlb.0905496.
22. Tulic MK, Piche T, Verhasselt V. Lung-gut cross-talk: evidence, mechanisms and implications for the mucosal inflammatory diseases. *Clin Exp Allergy* 2016;**46**:519–28. https://doi.org/10.1111/cea.12723.
23. Hind LE, Huttenlocher A. Neutrophil reverse migration and a chemokinetic resolution. *Dev Cell* 2018;**47**:404–5. https://doi.org/10.1016/j.devcel.2018.11.004.
24. Biasi F, Leonarduzzi G, Oteiza PI *et al.* Inflammatory bowel disease: mechanisms, redox considerations, and therapeutic targets. *Antioxid Redox Signal* 2013;**19**:1711–47. https://doi.org/10.1089/ars.2012.4530.
25. Zhou G, Yu L, Fang L *et al.* CD177(+) neutrophils as functionally activated neutrophils negatively regulate IBD. *Gut* 2018;**67**:1052–63. https://doi.org/10.1136/gutjnl-2016-313535.
26. Metzler KD, Goosmann C, Lubojemska A *et al.* A myeloperoxidase-containing complex regulates neutrophil elastase release and actin dynamics during NETosis. *Cell Rep* 2014;**8**:883–96. https://doi.org/10.1016/j.celrep.2014.06.044.
27. Eichele DD, Kharbanda KK. Dextran sodium sulfate colitis murine model: an indispensable tool for advancing our understanding of inflammatory bowel diseases pathogenesis. *World J Gastroenterol* 2017;**23**:6016–29. https://doi.org/10.3748/wjg.v23.i33.6016.
28. Chassaing B, Aitken JD, Malleshappa M *et al.* Dextran sulfate sodium (DSS)-induced colitis in mice. *Curr Protoc Immunol* 2014;**104**:15.25.1–15.25.14. https://doi.org/10.1002/0471142735.im1525s104.
29. Xu Q, Zhao W, Yan M *et al.* Neutrophil reverse migration. *J Inflamm (Lond)* 2022;**19**:22. https://doi.org/10.1186/s12950-022-00320-z.

Received 27 July 2024; revised 2 October 2024; accepted 12 October 2024. published 14 October 2024